VISCOELASTIC MEASUREMENT OF TRANSVERSE COMPLIANCE OF GLASS FIBER REINFORCED POLYMER COMPOSITES SPECIMENS

Skinner, Miles, and Mertiny, Pierre*
Department of Mechanical Engineering, University of Alberta, Edmonton, Alberta, Canada
* Corresponding author (pmertiny@ualberta.ca)

Keywords*: fiber-reinforced polymer composites, viscoelastic testing, creep, experimental procedure*

1 INTRODUCTION

The application of filament-wound fiber-reinforced polymer composites (FRPC) to the construction of flywheel rotors for energy storage has been a common practice for over 40 years and the study of composite material properties independent of application goes back even further [1]. Measurement methods for quasi-static elasticity are well documented [2-3], and well reported in literature [4-5], however documentation for viscoelastic material properties is less comprehensive. Moreover, due to the existence of edge effects, measurement of transverse viscoelastic compliance of unidirectional FRPC, such as those used in flywheel rotors, presents unique challenges for traditional coupon testing. Further, accurately measuring the anisotropic viscoelastic compliance of composite materials is critical to design and modeling of flywheel rotors [6-7]. Recognizing that FRPC that are filament-wound in the hoop direction are transversely isotropic [8-9], axial testing of tubular specimen is postulated to accurately represent the axial and radial transverse elasticity of thick-walled cylinders, such as those used in the construction of multi-rim flywheel rotors [10].

Skinner and Mertiny [7] showed that accounting for viscoelastic compliance is critical for designing and modeling composite flywheel rotors throughout their expected lifetime. The same is true for any application requiring long-term prediction of composite material behavior. Specifically, it is necessary to determine the compliance master curve of the material for its entire lifetime. ASTM D2990 [11] states the creep strain of a composite specimen can be found by heating test specimens to an elevated temperature while applying a known load and measuring creep strain. Then, viscoelastic compliance is calculated from creep strain using the known stress. Typically, the compliance master curve is constructed using employing the time-temperature superposition (TTSP) approach which relates short-term high temperature compliance with long-term low temperature compliance by shifting the short-term compliance measurements along a *log*(time) abscissa [12]. The shifting factors are commonly determined applying an Arrhenius equation using the empirically derived creep activation energy [13-14]. However, this method requires an additional set of experiments, to determine the activation energy, and may not be feasible. Other methods for determining shifting factors have been described in literature including the computational algorithm discussed in [15].

This article presents a low-cost experimental platform capable of conducting viscoelastic testing on thin-walled filament-wound FRPC tubular specimens with the goal of constructing the transverse compliance master curve. The experimental platform and specimens are discussed in detail including the data acquisition system, sensors, and testing procedure. Additionally, the validation of data processing and test platform is presented. The objective of this paper is to document the method for determining the compliance master curve of filament-wound composite specimens and reduce the barrier to entry for future researchers. The present study is conducted with glass fiber reinforced polymer composites (GFRP); however, the experimental platform and methodology is appropriate for any transversely isotropic material.

2 EXPERIMENTAL SETUP AND METHODOLOGY

2.1 Specimens

As shown in Figure 1, specimens comprise a composite tube and two aluminum tabs machined from 6061 aluminum. Tubes were filament-wound using glass fiber filament (Advantex Type 30, Owens Corning, Toledo, OH, USA) [16] onto a steel mandrel with a diameter of 25.4 mm. The matrix was a two-part epoxy (EPON 826 resin and EPIKURE 9551 hardener, Hexion, Columbus, OH, USA) [17] with a mixing ratio of 100:36. Table 1 gives further information on the composite material system and winding parameters. The winding angle was 88° to closely approximate a circumferential fiber orientation.

After winding, the resulting tubular part was cured on the rotating mandrel in an oven at 80°C for 1 hour, followed by 120°C for 2.5 hours. Tubes were then cut to length using a diamond saw. In preparation for adhesive bonding the tabs, the tube extremities were abraded and cleaned to create a uniform bonding surface. Prior to bonding, tubes and tabs were dried in an oven at 50°C, then the adhesive (DP460, 3M, Maplewood, MN, USA) was applied to bond the tabs to the tubes. Tubes and tabs were kept in alignment during room temperature cure using an alignment jig.

As manufactured, the composite tubes have a thin resin-rich area on the outer surface of the specimen. This layer contributes only marginally to the sample stiffness, so an effective wall thickness was used for analyses using the method described in [18]. In this method the effective wall thickness is found from the volume of the deposited fiber material and the fiber volume fraction, according to equations Eq.(1). The fiber volume fraction, v_f, was found by performing burn-out tests using five composite tube sections collected when cutting the specimens to length. The fiber volume fraction was found to be 0.667, yielding an effective wall thickness of 2.88 mm, which agrees well with the measured wall thickness of 3 mm, assuming a resin-rich surface layer of about 0.1 mm.

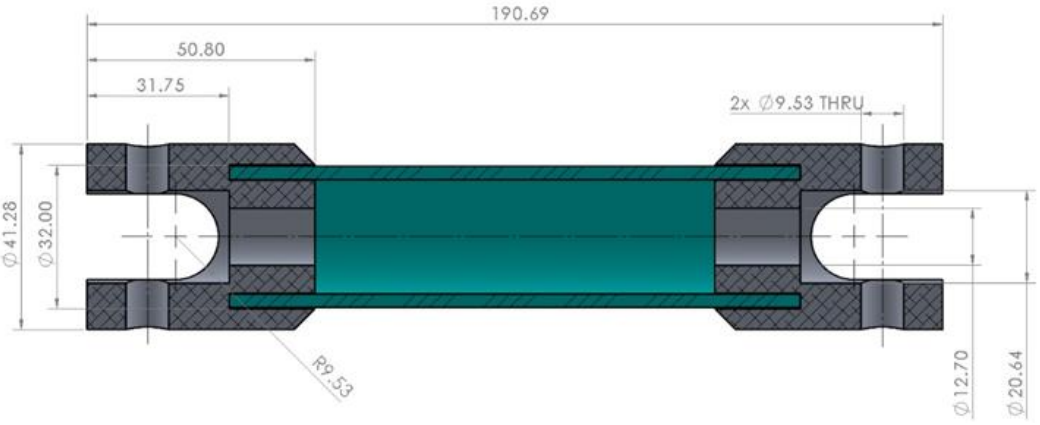

Figure 1. Cross-sectional diagram of test specimen assembly (dimensions in mm).

Table 1. Material system and winding parameters used to create composite tubes [16-17].

Property	Value
Fiber density, ρ_f	2560 kg/m^3
Matrix density, ρ_m	1160 kg/m^3
Linear density of fiber tow, *TEX*	0.735 g/m
Number of fiber tows, *TOW*	2
Winding circuits, *C*	1
Winding angle, α	88°
Number of layers, *N*	5
Inner diameter of composite tube, *ID*	25.4 mm

$$s = \sum_{n=1}^{N} t_{cover_n} \text{ where } t_{cover_n} = \frac{(TEX)(TOW)C}{\nu_f \rho_f \pi \left(\frac{ID}{2} + \sum_{i=1}^{n-1} t_{cover_i}\right) \cos(\alpha)} \quad (1)$$

2.2 Testing Equipment

An experimental setup was designed to satisfy the requirements established by ASTM D2990-17 [11]. Figure 2 depicts a diagram of the setup, consisting of a base, a support frame, a load cell, a mounted specimen, and lever arm with attached weight.

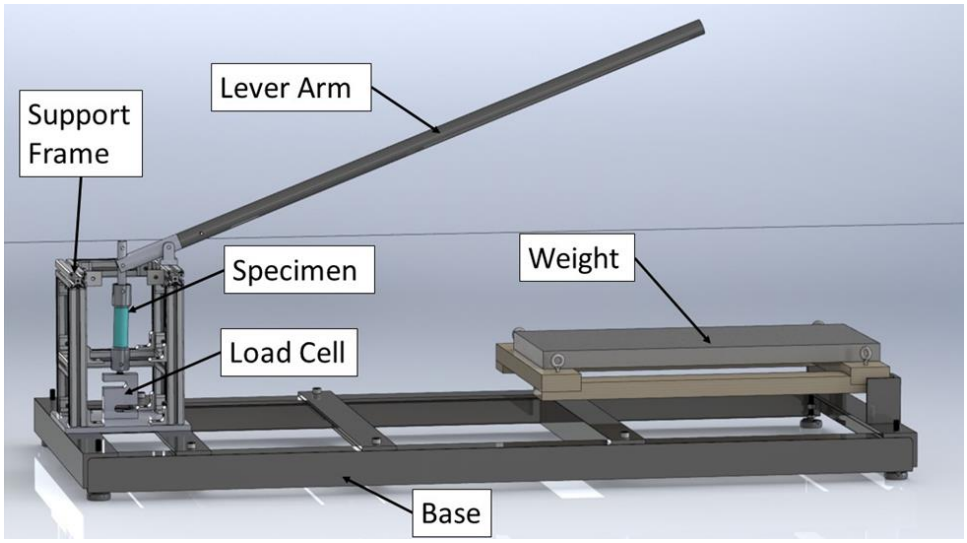

Figure 2. Diagram of creep test setup with labeled components. Some horizontal spars in the support frame have been hidden to provide an unobstructed view of the specimen and load cell.

2.2.1 Base and Support Frame

The steel base rests on four rubberized feet which prevent slipping and help insulate the platform from vibrations from nearby equipment. The base is bolted rather than welded together, allowing it to be disassembled and transported from the manufacturing to the testing location. A support frame is bolted to one end of the base, providing mounting points for the lever arm, the load cell, and mounting a specimen. The frame is constructed from T-slotted extruded aluminum bars, which provides the required strength and stiffness to support the forces required for loading the specimen. All base and frame components are relatively inexpensive and easy to machine, both of which reduces the costs for the platform. The lever arm is a thick-walled steel tube mounted to the top of the support frame with a mounting block. The long arm of the lever is 1,220 mm while the short arm is 116 mm, providing an as-manufactured mechanical advantage of 10.5:1. Load is applied by a weight suspended from the lever arm with four steel cables (not shown). The weight and its lifting structure are raised and lowered using a manual scissor jack (not shown).

2.2.2 Specimen Mounts

The specimen is affixed in the load train with 4.76 mm (3/16 inch) steel pins slip fit in the specimen tabs and tensile machine fixtures. This allows the specimen to rotate freely in the machine and minimize off-axis loading.

2.2.3 Heating Chamber

The specimen can be placed inside a heating chamber, which gently heats the specimen and maintains it at the desired temperature. Figure 3a shows a schematic of the heating unit assembled with a specimen. Heat is supplied by a custom silicone strip heater (Wattco Inc., LaSalle, QC, Canada) wrapped around a cylindrical steel housing. The top, bottom, and outside of the cylinder is insulated with fiberglass insulation.

2.2.4 Instrumentation and Data Acquisition Equipment

Specimens are instrumented with three types of sensors: strain gauges, a load cell, and a thermocouple. Diagrams for the data acquisition (DAQ) system and all sensors are provided in Figure 4. The load cell is an S-type load cell (type LC103B-5k, Omega Engineering, Norwalk, CT, USA).

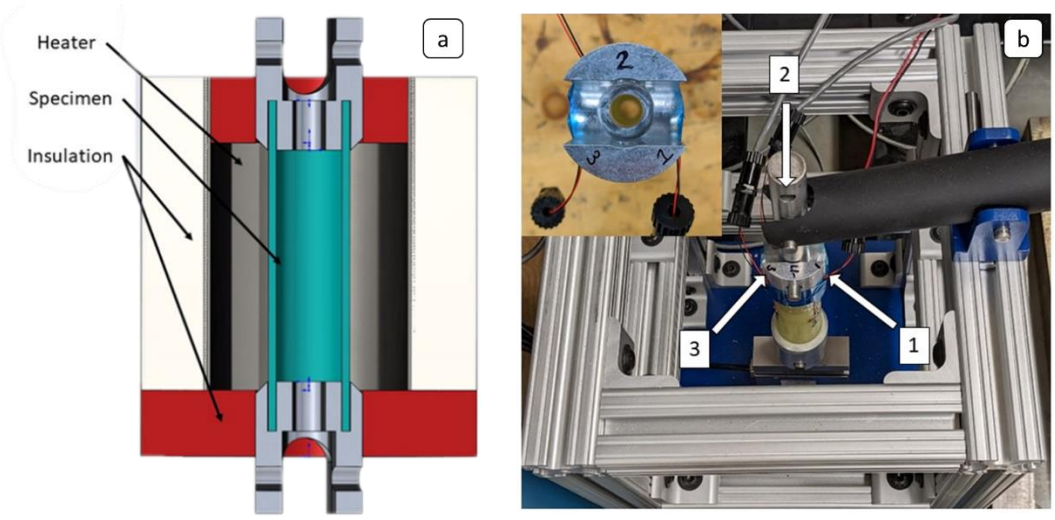

Figure 3. (a) Cross section of heating chamber and specimen, and (b) tensile machine showing specimen orientation (Inset: top-down view on specimen with strain gauges set up approximately 120° apart for viscoelastic experiments).

The strain gauge setup was altered between initial quasi-static and later viscoelastic testing in response to issues encountered during the former. Due to the possibility of off-axis loading creating bending stress in the sample, multiple strain gauges were attached to each sample. For quasi-static testing two strain gauges were applied to the surface of each sample approximately 90° apart. During quasi-static testing, off axis loading proved to be a reasonable concern so three strain gauges applied approximately 120° apart were used for creep testing. Hence, strain is collected from three independent gauges with the objective to assess whether the specimen is subjected to bending. If bending occurs, the magnitude and direction of bending can be determined. Moreover, data from the three gauges can be averaged to compensate for bending effects, similarly to [19]. A photograph of the specimen and strain gauge setup is shown in Figure 3b.

Two different strain gauges have been used, i.e., a dual-grid gauge CEA-13-125WT-350 and a single-grid gauge CEA-13-500UW-350 (both types by Vishay Precision Group Inc., Raleigh, NC, USA) [20-21]. Gauges are attached to the specimen using M-Bond 200 strain gauge adhesive, and aligned transverse to the fiber direction. The dual-grid and single-grid gauge are wired in a half-bridge and quarter bridge configuration, respectively. The gauges are connected to a Vishay 2100 gauge conditioner [22], which is used to balance the gauges before testing and apply amplifier gain. The specimen temperature is recorded with a custom-built PID controller that continuously monitors the sample temperature with a thermocouple and regulates the heating power to control the temperature. Three K-type thermocouples (BQLRZ, Shenzhen, China) are used to measure the ambient, heater, and specimen temperatures throughout an experiment. The PID settings for the temperature controller are 0.1, 100, and 1.0 respectively.

During testing, specimen strain and temperature, and applied load are collected continuously over time, *t*, at a sample rate of 1 Hz, using the NI DAQExpress software in conjunction with a NI 6008-USB device (National Instruments, Austin, TX, USA).

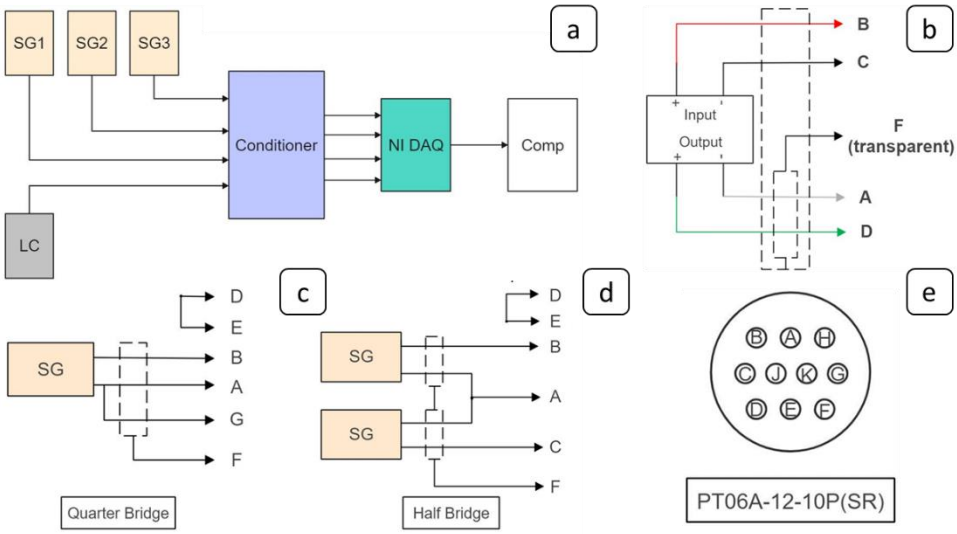

Figure 4: Instrumentation diagrams: (a) Schematic of sensors and data acquisition system; (b) circuit diagram for LC103B-5k load cell (color of leads corresponds to manufacturer setup); (c,d) circuit diagrams half- and quarter-bridge strain gauges; and (d) pin labels for gauge conditioner connector.

2.3 Experimental Procedures

2.3.1 Quasi-Static Testing

Quasi-static testing was performed using a universal testing machine (MTS 810, MTS, Eden Prairie, MN, USA) to determine the transverse tensile strength of GFRP specimens. Load was applied at 500 N/min until failure. Specimen strain was acquired with the sensor setup described above. Applied load and strain data were recorded by the control and DAQ computer of the testing machine.

2.3.2 Viscoelastic Testing

To determine the transverse compliance master curve of the material, a series of elevated temperature experiments (30°C, 45°C, 60°C) were performed at two applied loads. Testing at 30°C, rather than room temperature, was conducted to ensure a constant temperature can be maintained using the heater. The 45°C and 60°C settings were selected based on ASTM D2990 which stipulates characterizing a material over the useful temperature range in suitable increments that reflect creep variation with temperature and transitions of the material. The applied loads were set at 40% and 60% of the tensile strength (TS). Testing at 40% TS fosters significant creep deformation while minimizing the risk of crack initiation, as shown in [19] where limiting stress to below 50% TS was found improve fatigue performance.

The technical literature diverges on the need for specimen conditioning. In [23], conditioning was deemed necessary for measuring nonlinear viscoelasticity, while virgin specimens were used in [24] to directly measure linear viscoelastic behavior. Recognizing that time-temperature superposition is only valid for linear viscoelastic behavior, specimen conditioning was not performed.

After instrumenting and installing a specimen and starting the control and DAQ system, the testing procedure begins by heating the sample at the required temperature until it reaches equilibrium (2 hours). Note that test data is

recorded continuously during all stages of the experiment. Once at equilibrium, the first specified load is applied by engaging the weight in a steady manner using the scissor jack. The ensuing creep test stage runs for 30 minutes. Afterwards, the load is removed and the sample is heated to 75°C for 2 hours to allow for specimen recovery. This step is followed by equilibrizing the sample at the next required temperature. Then, the load is applied for the second creep test stage, again for 30 minutes. The recovery-heating-loading sequence is repeated in the same manner for the final temperature. Notice that strains are noted after each heating stage and before applying the load as this data is needed to separate thermo-mechanical from elastic and viscoelastic effects. A concern with the above procedure is using a single specimen for multiple creep test stages. However, this concern is alleviated by examining the recovery behavior. It has been shown that post-recovery strain of less than 5 με indicated minimal permanent damage, so the specimen could be used for the next treatment [19].

2.4 Data Reduction

Voltage signals recorded during the experiments were reduced to pertinent physical data. A linear voltage-force response was ascertaining for the load cell, allowing force and thus applied tensile stress to be determined using the specimen cross-sectional area. Recorded strain gauge data were isolated from the start to the end of each test stage. Gauge data from the quarter-bridge or half-bridge arrangement was converted to strain, ε, using Eqs.(2) and (3). Strain were then combined with applied stress to determine the time-dependent transverse compliance at each treatment temperature and load according to Eq.(4).

$$\varepsilon_{\text{quarter}}(t) = \frac{-4V_r(t)}{GF\left(1+2V_r(t)\right)}\left(1+\frac{R_{\text{L}}}{R_{\text{G}}}\right), \text{ or } \varepsilon_{\text{half}}(t) = \frac{-4V_r(t)}{GF[(1+\nu)-2V_r(t)(\nu-1)]}\left(1+\frac{R_{\text{L}}}{R_{\text{G}}}\right) \tag{2}$$

$$V_r(t) = \frac{V_{\text{strained}}(t) - V_{\text{unstrained}}(0)}{V_{\text{excitation}}}, \tag{3}$$

where R_{L} and R_{G} are correspondingly the lead wire and strain gauge resistance, *GF* is the gauge factor, *V* is the measured voltage, and *v* is the Poisson's ratio of the material (here, $R_{\text{L}} \approx 0$).

$$S_{22}(t) = \frac{\varepsilon(t)}{\sigma} \tag{4}$$

Employing TTSP the compliance master curve was constructed a employing shift factor, a_t. While there is no established convention for determining shift factors, it is common to calculate them using activation energy in an Arrhenius equation [26-27] or the Williams-Landel-Ferry equation [28-29]. However, this approach requires empirically determining the activation energy, which was not feasible in this study. Alternatively, the shift for each curve was determined analytically using the closed-form shifting algorithm described in [15], which determines the shift factor by minimizing the distance between the reference temperature compliance curve and the elevated temperature compliance data. Figure 5 illustrates this shifting algorithm. Consider two datasets, G_k and G_{k+1}, recorded at different temperatures, T_k and T_{k+1}, where each set contains *N* elements. Notably, *G* may denote any dataset, for example, creep strain data. The objective is to shift G_{k+1} along the abscissa to create a smooth curve. To accomplish this, the overlapping region from each data set is identified and used to define the boundaries of an overlapping window. These overlapping regions are

$$U_{k+1} = \left\{\log G_{k+1,n}\,, \log t_{k+1,n}\,, n = 1,2,..u_{k+1}\right\}, \tag{5}$$

$$L_k = \left\{\log G_{k,n}\,, \log t_{k,n}\,, n = l_k, l_{k+1}, N_k\right\}. \tag{6}$$

The location of the last point U_{k+1} is defined by an abscissa parallelpassing through the last point in G_k, and intersecting G_{k+1}. Similarly, the first point in L_k is defined by an abscissa parallel containing the first point in G_{k+1} and intersecting G_k. With the overlapping window defined, a_{k+1} is found by minimizing the area of this window. Hence,

$$A = A_k - A_{k+1} = 0 \tag{7}$$

$$\text{where } A_k = \sum_{n=L_k}^{N_k-1} \left[\frac{\log t_{k,n+1} + \log t_{k,n}}{2} \left(\log G_{k,n+1} - \log G_{k,n} \right) \right]. \tag{8}$$

Using Eqs.(7) and (8), the shift factor for the segment dataset measured at T_{k+1} is,

$$\log a_{k+1} = \frac{A_k - \sum_{n=1}^{U_{k+1}-1} \left[\frac{\log t_{k+1,n+1} + \log t_{k+1,n}}{2} \left(\log G_{k+1,n+1} - \log G_{k+1,n} \right) \right]}{\log G_{k,N_k} - \log G_{k+1,1}} \tag{9}$$

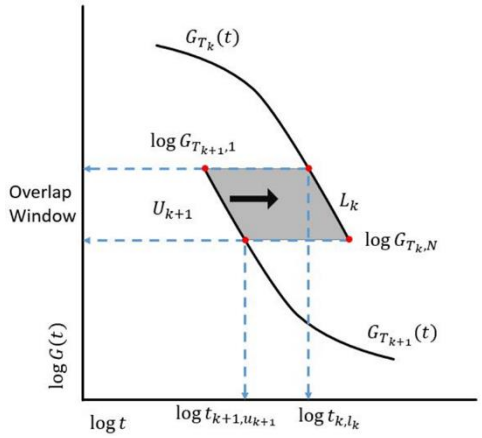

Figure 5: Schematic of data shifting procedure for compliance master curve.

There are several factors that affect the goodness of the shift resulting from the algorithm. It is important to control these factors to minimize shift errors. First, considering the size of the overlap window. Errors can be reduced by increasing the number of elements in the two overlap regions and the duration of the reference time in the window, both of which can be achieved by increasing the experiment duration. Second, considering the slope of the overlap regions, the error is minimized for moderately sloped overlapping regions and increases as the slope decreases toward zero and toward infinity. It has been shown in [15] that the ideal slope is approximately 0.05. The third and fourth factor for reducing shift errors are the magnitude of the experimental error that is controlled by the experimental setup, and the number of discrete data points per time unit in the reference frame, respectively.

The first step to applying the shift algorithm to the compliance data collected at the various temperatures is to select the lowest temperature as the reference temperature, T_k. The compliance at the next temperature T_{k+1} is shifted onto the reference temperature. Then, the two datasets are combined into a larger combined compliance, yielding the master curve at the reference temperature. Accordingly, the compliance at subsequent temperatures is shifted onto the master curve and added to the combined dataset. The master curve is complete when all elevated temperature compliance datasets have been shifted to the reference temperature. The final step is to determine a best fit equation that can be used to reproduce the master curve for the life of the material. Findley's power law is a common empirical model used to predict time-dependent compliance and creep of fiber reinforced polymer composites [30-31]. In terms of compliance, Findley's power law is written as

$$S_{22} = S_0 + At^n \tag{12}$$

where S_0 is the initial elastic compliance, and A and n are material constants. In the current study, curve fitting was performed using the built-in fitting tools in the Matlab programming environment (MathWorks, Natick, MA, USA).

3 Validation of Experimental Procedures

3.1 Applied Load and Temperature

Preliminary testing with a target load of 5,000 N was performed to validate the applied loading. A mass of 43.1 kg was suspended 122 cm from the fulcrum. The steel lever, inclined at approximately 15° from horizontal, imposes a mass of 2.52 kg at its half-length (66.5 cm). For the mechanical advantage of 10.5:1, the predicted force applied to the specimen is 4,577 N compared to the load cell measurement 4,593 N ± 7 N, yielding an error of 0.3%. Figure 6a confirms that the applied loading is constant without drift.

The controller for the heater measures the chamber temperature and the specimen surface temperature. The latter is used for control purposes. The graph in Figure 6b depicts the surface and chamber temperatures for a 3-hour experiment. Notably, the chamber temperature is 55°C for a target specimen surface temperature 45°C. The graph confirms that the heater closely maintains the desired specimen temperature after about 2 hours of equilibrizing.

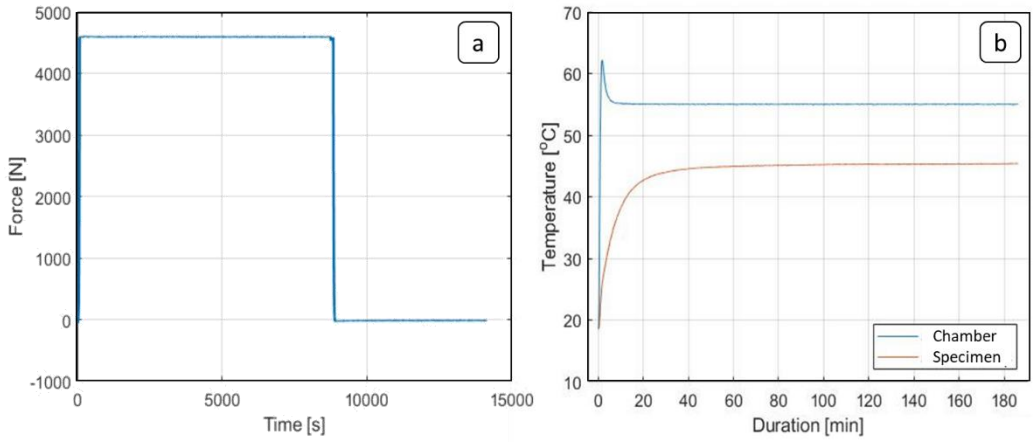

Figure 6: Data for test equipment validation: (a) Specimen surface and chamber temperatures for a 3-hour experiment, and (b) load cell readings for applied load.

3.2 Strain Measurements and Bending Effects

In some instances, during quasi-static testing, differences in strain readings were observed between the three gauge locations along the specimen circumference, presumably due to bending effects. Example strain data is shown in Figure 7a, where gauges 1 and 3 recorded the largest strain indicating these gauges are on the outside of the bend radius while gauge 2 shows the least strain indicating it is on the inside of the bend radius. From a top-down perspective, the specimen is bending as indicated by the inset in Figure 7a. Bending is thought to originate from misalignment, either from imperfect mounting the specimen in the machine and/or a lack of cylindrical concentricity between specimen tube and metallic end tabs. Misalignments effects can be corrected by changing the specimen, or as mentioned above, by employing a procedure for compensating for bending effects as described in e.g. [19].

Figure 7b depicts sample creep strain data for a specimen subjected to the load described above. The strain measurements from each strain gauge have been averaged together to compensate for off-axis loading as discussed. The elastic strain caused by quasi-static loading and the recovery data have been removed from this graph to better display the creep strain results. The small discontinuity seen at 6,000 s is possibly due to a material defect or failure. The data in Figure 7b confirms the capability of the developed test setup and procedure to yield the transverse compliance master curve for FRPC specimens.

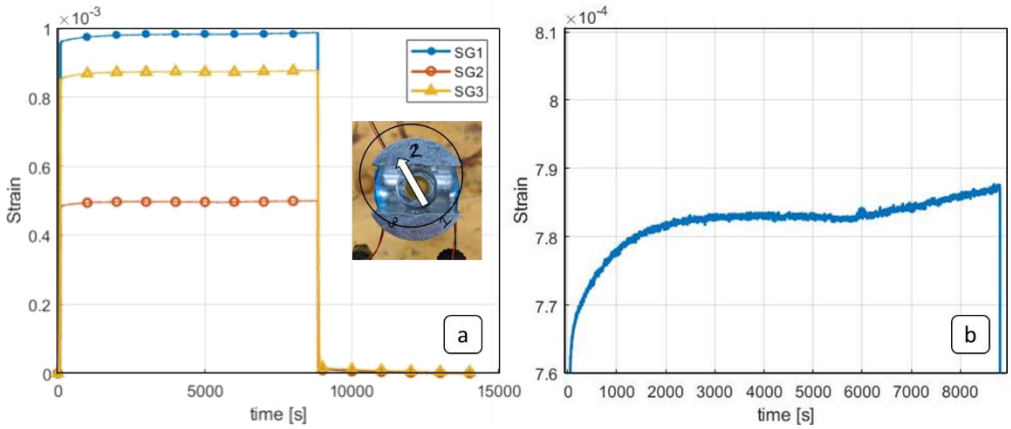

Figure 7: (a) Difference between strain data from strain gauges (SG) due to bending stress (Inset: Arrow indicating specimen bending direction from off axis loading), and (b) sample creep strain data.

4 Conclusion

Determining the transverse viscoelastic compliance master curve for FRPC presents unique challenges for traditional coupon testing due the existence of edge effects. Additionally, testing requirements, specimen preparation, and data collection and processing are significant challenges to overcome. This article presented an experimental test platform and process capable of conducting elevated temperature testing employing tubular filament-wound FRPC specimens. Specimen discussed herein were made from glass-fiber/epoxy composites with circumferential fiber orientation. The specimen fabrication parameters and experimental methods for viscoelastic material characterization were discussed in detail. The process for constructing the compliance master curve from collected creep strain data was described. Finally, the performance of the experimental setup was validated, confirming its ability to apply the desired loads and temperatures while recording pertinent data for computing stress and strain. It was observed that off-axis loading (bending) may be a concern, however, its effects can be accounted for during data processing. In closing, the experimental platform along with the methodology for conducting viscoelastic material testing was ascertained to successfully yield the data required for constructing the transverse compliance master curve for FRPC specimens.

5 REFERENCES

[1] M. Skinner and P. Mertiny, “Energy Storage Flywheel Rotors—Mechanical Design,” *Encyclopedia*, vol. 2, no. 1, pp. 301–324, 2022.

[2] ASTM, “ASTM D3039/D3039M,” pp. 1–13, 2014.

[3] ASTM, “ASTM D7205,” pp. 1–13, 2011.

[4] M. Y. Khalid, A. Al Rashid, Z. U. Arif, N. Akram, H. Arshad, and F. P. G. Márquez, “Characterization of failure strain in fiber reinforced composites: Under on-axis and off-axis loading,” *Crystals*, vol. 11, no. 2, pp. 1–11, 2021.

[5] A. Saleeb, S. Arnold and N. Al-Zoubi, “A study of time-dependent and anisotropic effects on the deformation response of two flywheel designs,” *ASTM Spec. Tech. Publ.*, no. 1436, pp. 1–27, 2003.

[6] J. T. Tzeng, “Viscoelastic Analysis of Composite Cylinders Subjected to Rotation,” *Trans. Ophthalmol. Soc. U. K.*, vol. 101, no. 2, pp. 200–202, 2001.

[7] M. Skinner and P. Mertiny, “Effects of Viscoelasticity on the Stress Evolution over the Lifetime of Filament-Wound Composite Flywheel Rotors for Energy Storage,” *Appl. Sci.*, vol. 11, no. 20, p. 9544, 2021.

[8] H. Ding, W. Chen and Z. L., Elasticity of Transversely Isotropic Materials. Springer, 2006.

[9] L. Di Gennaro, F. Daghia, M. Olive, F. Jacquemin, and D. Espinassou, “A new mechanism-based temperature-dependent viscoelastic model for unidirectional polymer matrix composites based on Cartan decomposition,” *Eur. J. Mech. A/Solids*, vol. 90, p. 104364, 2021.

[10] M. Skinner and P. Mertiny, “Experimental Characterization of Low-Speed Passive Discharge Losses of a Flywheel Energy Storage System,” *Appl. Mech.*, vol. 2, no. 1, pp. 1–15, 2021.

[11] ASTM, “ASTM D2990-09,” pp. 1–20, 2009.

[12] S. Sihn and S. Tsai, “Automated shift for time-temperature superposition,” *Proceedings of 12th Int. Com. Compos. Mater.*, p. 51, 1999.

[13] B. T. Werner and K. Nelson, “Time Temperature Superposition Shift Factors for Fabric Composites,” *Proceedings of Proc. Soc. Exp. Mech. Ser.*, pp. 95–98, 2021.

[14] N. Nosrati, A. Zabett, and S. Sahebian, “Long-term creep behaviour of E-glass/epoxy composite: time-temperature superposition principle,” *Plast. Rubber Compos.*, vol. 49, no. 6, pp. 254–262, 2020.

[15] M. Gergesova, B. Zupančič, I. Saprunov, and I. Emri, “The closed form t-T-P shifting (CFS) algorithm,” *J. Rheol.*, vol. 55, no. 1, pp. 1–16, 2011.

[16] Owens Corning, “SE12000 Single-End Type 30 Roving,” 2019.

[17] Hexion, “EPON Resin 826 Technical Data Sheet,” 2005.

[18] P. Mertiny and F. Ellyin, “Influence of the filament winding tension on physical and mechanical properties of reinforced composites,” *Compos. Part A Appl. Sci. Manuf.*, vol. 33, no. 12, pp. 1615–1622, 2002.

[19] R. P. Emerson, “Viscoelastic Flywheel Rotors: Modeling and Measurement,” Pennsylvania State University, 2002.

[20] Vishary Precision Group, “General Purpose Strain Gages 500UW,” 2018.

[21] Vishary Precision Group, “General Purpose Strain Gages 125WT — Tee Rosette,” 2015.

[22] Vishay Precision Group, “Vishay 2100 Strain Gauge Conditioner-Amplifier System.” pp. 1–9

[23] Y. C. Lou, “Viscoelastic Characterization of Nonlinear Fiber-Reinforced Plastic,” *J. Compos. Mater.*, vol. 5, pp. 208–234, 1971.

[24] Y. Y. T. Yeow, D. D. H. Morris, and H. H. F. Brinson, “The Time-Temperature Behavior of a Unidirectional Graphite/Epoxy Composite,” *Fifth Conf. Compos. Mater. Test. Des.*, pp. 263–19, 1979.

[25] J. L. Sullivan, E. J. Blais, and D. Houston, “Physical aging in the creep behavior of thermosetting and thermoplastic composites,” *Compos. Sci. Technol.*, vol. 47, no. 4, pp. 389–403, 1993.

[26] M. Durante, A. Formisano, L. Boccarusso, A. Langella, and L. Carrino, “Creep behaviour of polylactic acid reinforced by woven hemp fabric,” *Compos. Part B Eng.*, vol. 124, pp. 16–22, 2017.

[27] C. M. Wu, P. C. Lin, and R. Murakami, “Long-term creep behavior of self-reinforced PET composites,” *Express Polym. Lett.*, vol. 11, no. 10, pp. 820–831, 2017.

[28] M. L. Williams, R. F. Landel, and J. D. Ferry, “The Temperature Dependence of Relaxation Mechanisms in Amorphous Polymers and Other Glass-forming Liquids,” *J. Am. Chem. Soc.*, vol. 77, no. 14, pp. 3701–3707, 1955.

[29] A. Koutsomichalis, T. Kalampoukas, and D. E. Mouzakis, “Mechanical testing and modeling of the time–temperature superposition response in hybrid fiber reinforced composites,” *Polymers (Basel).*, vol. 13, no. 7, 2021.

[30] N. P. Lorandi, M. O. H. Cioffi, C. Shigue, and H. L. Ornaghi, “On the creep behavior of carbon/epoxy non-crimp fabric composites,” *Mater. Res.*, vol. 21, no. 3, pp. 1–8, 2018.

[31] D. C. T. Cardoso and K. A. Harries, “A viscoelastic model for time-dependent behavior of pultruded GFRP,” *Constr. Build. Mater.*, vol. 208, pp. 63–74, 2019.